taining domatia-bearing leaves and in a leaf domatium of *Sarcopteryx* sp. aff. *martyana* (Sapindaceae) from stream channels under CNVF at Noah Creek.

The discovery of acarodomatia and mites from Eocene deposits separated by over 600 km suggests that mite-plant associations were widespread in rain forest across southern Australia over 40 million years ago. Both deposits contain fossil oribatids with arboreal features, the same domatia-bearing leaf taxa occur in similar frequencies, and leaf physiognomy and the frequency of domatia-bearing leaf types are comparable to present-day CNVF (*9, 16*). Acarodomatia and mites should also occur in Tertiary deposits in other regions (*17*). Up to 50% of present-day genera of woody plants in deciduous broadleaf forest have domatia (*6, 18*) and many, such as *Acer, Juglans, Quercus, Tilia*, and *Ulmus*, are important elements in Tertiary floras (*19*).

The radiation of epiphyllous and parasitic fungi (*20*) and phytophagous arthropods (*21*) that accompanied the diversification of angiosperms may help explain the occurrence of acarodomatia by the Eocene. At least seven taxa of epiphyllous fungi occur on Eocene leaves at AN and GG (*22*), and they are present in Tertiary floras elsewhere in Australia (*23*). Insects also mined Elaeocarpaceous leaves (*24*), and phytophagous mites are associated with Eocene leaves at a nearby site (*25*). These types of antagonistic interactions probably led to the early diversification of defenses among angiosperms (*21, 26*). Our results suggest that protective mutualism between arthropods and plants may be ancient.

REFERENCES AND NOTES

1. W. Crepet, *Rev. Palaeobot. Palynol.* **27**, 213 (1979); J. Basinger and D. Dilcher, *Science* **224**, 511 (1984).
2. A. Beattie, *The Evolutionary Ecology of Ant-Plant Mutualisms* (Cambridge Univ. Press, Cambridge, 1985), p. 8.
3. A. Lundström, *Nova Acta Reg. Soc. Uppsala* **3**, XIII (1887).
4. P. Kevan, W. Chaloner, D. Savile, *Paleontology* **18**, 391 (1975); W. Shear *et al.*, *Science* **224**, 492 (1984); G. Krantz, *A Manual of Acarology* (Oregon State Univ. Press, Corvallis, 1986), p. 1.
5. D. O'Dowd and M. Willson, *Biol. J. Linn. Soc.* **37**, 191 (1989).
6. R. Pemberton and C. Turner, *Am. J. Bot.* **76**, 105 (1989).
7. Mummified leaves are a rare form of fossilization in which the cuticular envelope of the leaf remains intact.
8. D. Christophel, W. Harris, A. Syber, *Alcheringa* **11**, 303 (1987); D. Christophel and D. Greenwood, *Trans. R. Soc. S. Aust.* **111**, 155 (1987).
9. D. Christophel and D. Greenwood, *Proc. Ecol. Soc. Aust.* **15**, 139 (1988). Notophyllous leaves are 7.5 to 12.5 cm in length [L. Webb, *J. Ecol.* **47**, 551 (1959)].
10. No set of foliar characters distinguishes between *Elaeocarpus* and *Sloanea* species at the generic level. The entire margined taxon can be confidently placed with the Lauraceae [R. Hill, *Alcheringa* **10**, 327 (1986)].
11. Domatia number per leaf averaged 8.8, 12.8, and 9.4 on *S. australis* subsp. *parviflora, S. langii*, and *S. woolsii*.
12. J. Aoki, *Pacif. Sci.* **8**, 281 (1966); R. Norton, *Acarologia* **24**, 449 (1983); R. Norton and J. Palacios-Vargas, *ibid.* **28**, 75 (1987); C. Perez-Inigo, *Graellsia* **43**, 127 (1987); D. Lee and C. Birchby, *Trans. R. Soc. S. Aust.* **113**, 1 (1989).
13. J. Aoki, *3rd Int. Congr. Acarol.* (1971), p. 59. The bothridial sensillus may be an air-current (rheotactic) receptor. The elaborate forms in the soil-litter environment may be unnecessary in an exposed environment where the sensillum is usually shortened and near globose [R. Norton and J. Palacios-Vargas, *Folia Entomol. Mex.* **52**, 61 (1982)].
14. E. Seyd and M. Seaward, *Zool. J. Linn. Soc.* **80**, 369 (1984).
15. A total of 2996 domatia, 547 leaves, and 102 shoots on 19 trees was sampled. Mites occupied 27 to 88% of the domatia of each species.
16. At AN and GG, 2 of 18 and 2 of 25 leaf types have domatia, respectively. At Noah Creek, 2 of 27 leaf types in leaf litter on the forest floor had acarodomatia; in leaf litter packs from the stream channel, 3 of 30 and 4 of 32 had domatia.
17. A. Lundström, *Bot. Zentblatt.* **14**, 246 (1890).
18. Y. Brouwer and H. Clifford, *Notes Jodrell Lab.* **12**, 1 (1990); M. Willson, unpublished results.
19. O. Ball, *Bull. Agric. Mech. Coll. Texas* **2**, 1 (1931); J. Wolfe, in *Paleobotany, Paleoecology, and Evolution*, K. Niklas, Ed. (Praeger, New York, 1981), vol. 2, p. 79.
20. D. Dilcher, *Paleontographica* **116**, 1 (1965); K. Pirozynski, *Annu. Rev. Phytopath.* **14**, 237 (1976).
21. P. Ehrlich and P. Raven, *Evolution* **18**, 586 (1964).
22. D. Christophel, unpublished results.
23. R. Lange, *N. Jb. Geol. Palaont. Abh.* **151**, 142 (1976).
24. A. Rozefelds, *Alcheringa* **12**, 1 (1988).
25. R. Southcott and R. Lange, *Rec. S. Aust. Mus.* **16**, 1 (1971).
26. P. Regal, *Science* **196**, 622 (1977).
27. Mites were extracted using the Na_2CO_3 method [M. Brasier, *Microfossils* (Allen & Unwin, London, 1980), p. 164].
28. D. Christophel and S. Lys, *Aust. J. Bot.* **34**, 649 (1986).

29. A. Irvine, B. Gray, R. Halliday, D. Lee, S. Swann, M. Willson, and N. Wilson helped with the study. A. Beattie, B. Downes, R. Halliday, E. Lindquist, D. Walter, and M. Willson improved the manuscript. Supported by the Australian Research Council.

30 July 1990; accepted 9 January 1991

Strain Measurements and the Potential for a Great Subduction Earthquake Off the Coast of Washington

J. C. SAVAGE* AND M. LISOWSKI

Geodetic measurements of deformation in northwestern Washington indicate that strain is accumulating at a rate close to that predicted by a model of the Cascadia subduction zone in which the plate interface underlying the continental slope and outer continental shelf is currently locked but the remainder of the interface slips continuously. Presumably this locked segment will eventually rupture in a great thrust earthquake with a down-dip extent greater than 100 kilometers.

THE POTENTIAL FOR A GREAT THRUST earthquake in the Cascadia subduction zone along the coast of Washington (Fig. 1) has been a subject of controversy (*1*). The Juan de Fuca plate is being subducted beneath the North American plate in an east-northeastward direction. Subduction there may be aseismic, that is, incapable of producing a great earthquake. The absence of even small thrust earthquakes along the plate interface is the primary evidence for aseismic subduction (*2*). That evidence is supported to some extent by indications that the shallow regional stress field in northwestern Washington involves north-northeast compression (*3*) rather than the east-northeast compression expected from subduction. The relative youth (~8 million years) and the thick sediment cover of the oceanic plate at the deformation front imply high temperatures in the subducted plate and high pore pressures in the subducted sediments and overlying accretionary prism, conditions that favor aseismic subduction (*4, 5*). However, great earthquakes do occur at other subduction zones where relatively young ocean crust is blanketed by a thick sediment cover (*6*), and geologic evidence (*7, 8*) indicates that large earthquakes have occurred along the coast of Washington at an average interval of about 600 years over the past several thousand years. Also, resurveys of triangulation and trilateration networks (*9*) generally indicate an east-northeast contraction in northwestern Washington consistent with the accumulation of strain expected for seismic subduction.

To obtain an accurate measure of strain accumulation along the Cascadia subduction zone, we installed an eight-station trilateration network (Fig. 1) in the eastern core of the Olympic terrane, a post-Eocene accretionary prism. The network was surveyed in September 1982, 1983, 1986, and 1990. In each survey the same 21 distances between pairs of geodetic stations were measured with a Geodolite, a precise electro-optical distance-measuring instrument. The refractivity correction was determined from endpoint pressure measurements and temperature and humidity profiles measured along the line from a small aircraft at the time of ranging (*10*). The measured distances range from 9 to 27 km, and the standard errors in

U.S. Geological Survey, 345 Middlefield Road, Mail Stop 977, Menlo Park, CA 94025.

*To whom correspondence should be addressed.

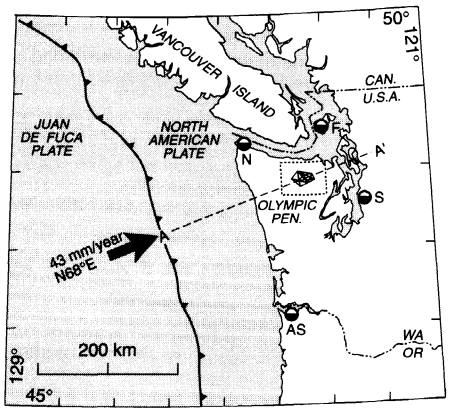

Fig. 1. Map of the Cascadia subduction zone showing the location of the Olympic trilateration network (within dashed rectangle) and four tide gages (half-filled circles identified as follows: AS, Astoria; F, Friday Harbor; N, Neah Bay; S, Seattle). The sinuous barbed line locates the deformation front, which lies at the base of the continental slope.

Table 1. Rebound corrected uplift rates inferred from the 1940 to 1975 average rate of relative sea-level (RSL) rise. Eustatic rate is 2.4 ± 0.9 mm/year. Uncertainties are standard errors.

Tide gage	Rate of RSL rise (mm/year)	Rebound (mm/year)	Tectonic uplift rate (mm/year)
	Outer coast		
Astoria	−0.7 ± 0.6	−0.7	3.8 ± 1.2
Neah Bay	−1.7 ± 0.5	−0.0	4.1 ± 1.1
	Inland		
Friday Harbor	0.6 ± 0.5	1.1	0.7 ± 1.1
Seattle	2.3 ± 0.5	0.7	−0.6 ± 1.1

those measurements increase with distance from 3.5 to 6.2 mm.

The average rate of strain accumulation in the Olympic network from 1982 to 1990 can be estimated from the changes in distances measured in the trilateration surveys. The dimensions of the network (30 by 20 km) are sufficiently small compared to the dimensions of the subduction zone that strain accumulation within the network may be regarded as uniform. One then solves for the tensor strain rate, uniform in both space and time, that best explains the observed changes in line length (that is, distances between stations), taking account of the various orientations of the individual lines. The best-fit principal strain rates are $\dot{\epsilon}_1$ = 0.011 ± 0.027 and $\dot{\epsilon}_2$ = −0.092 ± 0.029 microstrain (μstrain) per year (extension reckoned positive) with the axis of greatest contraction directed N59°E ± 6.6°. That strain field is adequately described as an N59°E uniaxial contraction. The orientation of the contraction axis corresponds reasonably well with the N68°E direction of plate convergence expected for the Juan de Fuca–North American plate interaction (*11*). The extension rate for a line of length L and azimuth θ predicted by that field is

$$L^{-1}(dL/dt) = (\dot{\epsilon}_1 + \dot{\epsilon}_2)/2 + [(\dot{\epsilon}_1 - \dot{\epsilon}_2)/2]\cos 2(\theta - \phi) \quad (1)$$

where φ is the azimuth of principal extension, and $\dot{\epsilon}_1$ and $\dot{\epsilon}_2$($\dot{\epsilon}_1 > \dot{\epsilon}_2$) are the principal strain rates. The observed extension rate is $L^{-1}(dL/dt)$, where dL/dt is estimated from the slope of the linear fit to a plot of line length versus time. The fit of the predicted strain-rate solution to the extension rates observed along the 21 lines in the network is shown in Fig. 2. None of the observed extension rates differs by as much as 2 SD from the best-fit predicted extension rate.

Additional measurements of deformation along the Cascadia subduction zone are available in the form of uplift rates (Table 1) deduced from relative sea-level measurements at four tide gages (Fig. 1). The average rate of rise in relative sea level at a tide gage was taken as the slope of the linear fit to a plot of relative sea level versus time for the interval from 1940 to 1975 (*12*). We corrected this rate of rise for the eustatic rise in sea level (2.4 ± 0.9 mm/year) and the apparent rate of sea-level rise due to local glacial isostatic rebound (*13*) to obtain the local tectonic subsidence rate (Table 1).

In aseismic subduction the slip rate at the plate interface is equal to the plate convergence rate so that the underthrust plate slips steadily beneath the overthrust plate. Seismic subduction is attributed to locking of the shallow segment of the interface while steady slip continues on the remainder of the interface. The earthquake corresponds to rupture of the locked segment.

Interseismic deformation at a subduction zone is attributed to the slip deficit that accumulates on the locked segment of the plate interface and on the segment directly down dip where a partial slip deficit accumulates as a result of the pinning effect of the locked segment. A simple representation of the process is provided by a fault model in an elastic half-space. The fault represents the part of the plate interface where interseismic slip is inhibited by locking; this includes the locked zone itself and the interface segment

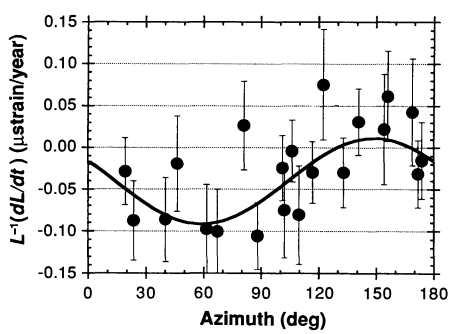

Fig. 2. Average extension rate along each of the lines in the Olympic network as a function of the azimuth of the line. The error bars represent 1 SD. The sinusoid represents the extension rates predicted by the best-fitting uniform strain field.

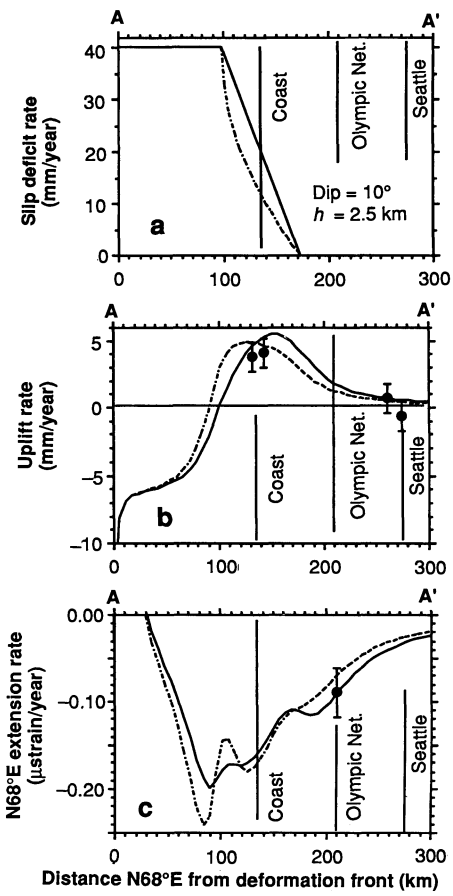

Fig. 3. Interseismic deformation rates resolved into extension rate (**c**) and uplift rate (**b**) predicted along the profile AA′ (Fig. 1) by simple models of subduction for the two distributions of slip-deficit rates shown in (**a**). The solid and dashed lines show the rates predicted for two different distributions of slip deficit. The abscissa shows the horizontal distance from the deformation front measured along the profile AA′. The plotted points show the observed deformation rates. Error bars represent 1 SD; h, depth below sea level of deformation front in model.

directly down dip. In the model, slip is imposed on this fault at a rate equal to the slip deficit accumulating on the plate interface. This slip, being a deficit, is in the opposite sense (that is, normal slip as opposed to thrust) to that occurring elsewhere on the plate interface. The surface deformation rates produced in the model are taken to represent the interseismic deformation rates observed on the overthrust plate (*14*).

The model fault for the Cascadia subduction zone off the Washington coast is specified as follows: The plate convergence rate is about 40 mm/year N68°E (*11*), and the fault dips 10° N68°E from the deformation front at the base of the continental slope (Fig. 1) at a depth of 2.5 km below sea level (*15*). Because the brittle-ductile transition on the fault occurs at a depth of about 20 km (*4*), the locked segment can extend only about 100 km down dip from the sea-floor trace at the deformation front. The slip deficit on this locked segment is equal to the plate convergence rate, 40 mm/year. Down dip from the locked segment is a transitional segment over which the slip deficit decreases from the full rate of 40 mm/year to zero. This transitional segment is a consequence of the elastic constraints limiting slip in the neighborhood of a pinned region (*16*). The transitional segment was arbitrarily assigned a 75-km down-dip dimension. We considered two arbitrary slip-deficit distributions (Fig. 3a) for the transitional segment of the plate interface, one in which the slip rate decreased linearly with down-dip distance and the other in which the decrease was proportional to the square root of that distance. The slip deficit was zero beyond 175 km down dip from the sea-floor trace (that is, at depths greater than 33 km). Finally, we assume that deformation is uniform in the direction of fault strike. The deformation rates predicted by the two different slip-deficit distributions (Fig. 3) assigned to the transitional segment of the plate interface are not significantly different at the level of observational precision.

The proposed model explains most of the observations relevant to the character of subduction at the Cascadia zone. The observed surface deformation rates (-0.089 ± 0.028 μstrain/year N68°E extension at the Olympic network, and uplift rates from Table 1) are in rough agreement with the rates predicted by the model (Fig. 3, b and c). Moreover, the shallow extent (maximum depth, 20 km) of the locked segment of the plate interface is consistent with the thermal constraints (*4*). The location of the locked segment beneath the continental slope and shelf implies that thrust events should occur offshore, where they are difficult to locate and identify, not beneath the Olympic Peninsula. Finally, rupture of the locked segment will produce the coastal coseismic subsidence inferred from the geologic record (*9*).

REFERENCES AND NOTES

1. G. C. Rogers, *Nature* **332**, 17 (1988); T. H. Heaton, *ibid.* **343**, 511 (1990).
2. J. J. Taber and S. W. Smith, *Bull. Seismol. Soc. Am.* **75**, 237 (1985).
3. R. S. Crosson, *ibid.* **62**, 1133 (1972); C. S. Weaver and S. W. Smith, *J. Geophys. Res.* **88**, 10371 (1983); M. L. Zoback, *U.S. Geol. Surv. Open-File Rep. 90-334* (1990), p. 537.
4. E. E. Davis, R. D. Hyndman, H. Villinger, *J. Geophys. Res.* **95**, 8869 (1990).
5. D. E. Byrne, D. M. Davis, L. R. Sykes, *Tectonics* 7, 833 (1988).
6. T. H. Heaton and S. H. Hartzell, *Science* **236**, 162 (1987).
7. J. Adams, *Tectonics* **9**, 569 (1990).
8. B. F. Atwater, *Science* **236**, 942 (1987).
9. J. C. Savage, M. Lisowski, W. H. Prescott, *J. Geophys. Res.* **86**, 4929 (1981); M. Lisowski, W. H. Prescott, H. Dragert, *Seismol. Res. Lett.* **60**, 1 (1989).
10. J. C. Savage and W. H. Prescott, *J. Geophys. Res.* **78**, 6001 (1973).
11. C. DeMets, R. G. Gordon, D. F. Argus, S. Stein, *Geophys. J. Int.* **101**, 425 (1990).
12. S. D. Hicks, *J. Geophys. Res.* **83**, 1377 (1978).
13. W. R. Peltier and A. M. Tushingham, *Science* **244**, 806 (1989); A. M. Tushingham and W. R. Peltier, *J. Geophys. Res.*, in press.
14. J. C. Savage, *J. Geophys. Res.* **88**, 4984 (1983).
15. J. J. Taber and B. T. R. Lewis, *Bull. Seismol. Soc. Am.* **76**, 1011 (1986).
16. J. Weertmann, *ibid.* **54**, 1035 (1964).

17. We thank the Superintendent of Olympic National Park for permitting surveys within the park and R. Weldon for a constructive review of the manuscript.

7 November 1990; accepted 7 February 1991

Approaches for Optimizing the First Electronic Hyperpolarizability of Conjugated Organic Molecules

S. R. MARDER, D. N. BERATAN, L.-T. CHENG

A two-state, four-orbital, independent electron analysis of the first optical molecular hyperpolarizability, β, leads to the prediction that |β| maximizes at a combination of donor and acceptor strengths for a given conjugated bridge. Molecular design strategies that focus on the energetic manipulations of the bridge states are proposed for the optimization of β. The limitations of molecular classes based on common bridge structures are highlighted and more promising candidates are described. Experimental results supporting the validity of this approach are presented.

SECOND-ORDER NONLINEAR OPTICAL properties, which are exploited in telecommunications, data storage, and information processing applications, arise in molecules that lack a center of symmetry (*1–4*). Such materials can be used to double the frequency of laser light or can be used in electrooptic switches, for example. Conjugated organic molecules with electron donating and accepting moieties can exhibit large electronic second-order nonlinearities (or first hyperpolarizabilities, β). In general, β increases with increasing donor and acceptor strength [related to the ionization potentials of the filled donor and empty acceptor orbitals or the coulomb energies of independent electron theory (*5*)] and with increasing separation so long as there is strong electronic coupling through the conjugated bridge.

The full perturbation theory expression for β has the form of a sum of contributions from all electronic states. However, for many donor-acceptor–substituted organics, such as 4-nitroaniline, a two-state approximation for β is adequate because the charge transfer (CT) excited-state term dominates the perturbation sum. The two-state expression for the dominant nonresonant component of the β tensor is proportional to:

$$(\mu_{ee} - \mu_{gg}) \frac{\mu_{ge}^2}{E_{ge}^2} \qquad (2)$$

where g is the index of the ground state, e is the index of the CT excited state, and μ is the dipole matrix element between the two subscripted states (*6*). For many organic molecules, the two-state expression accounts reasonably well for the experimental β values obtained by electric field–induced second harmonic generation (EFISH) measurements done in solution with a dc field (*7, 8*). Such experiments measure the vector projection of the hyperpolarizability tensor (β) along the molecular dipole (μ) direction. Although reservations exist for the general adequacy of the two-state approximation in extended molecules, it does capture the qualitative spectroscopic dependences of β for molecules with strong CT transitions. Simple molecular orbital considerations and the two-state approximation for β have been used to predict that a

S. R. Marder and D. N. Beratan, Jet Propulsion Laboratory, California Institute of Technology, Pasadena, CA 91109, and The Beckman Institute, California Institute of Technology, Pasadena, CA 91125.
L.-T. Cheng, E. I. DuPont de Nemours and Company, Inc., Wilmington, DE 19880–0238.